A Coupled CFD-DEM Numerical Simulation of the Behavior of Particles Bridging and Destabilization in Natural Fractures

Jiaxin Feng, Gao Li, Rui Li, and Yi Zhang

Abstract Lost circulation affects the safety and efficiency of drilling operations significantly, especially in naturally fractured formations. Adding granular lost circulation materials (LCMs) into the drilling fluid is the most commonly used to prevent/mitigate lost circulations. However, the bridging sealing mechanism of granular LCMs in natural fracture space is ambiguous at the meso-scale, which has limited its effectivity seriously. In order to investigate the bridging and destabilization behavior of rigid particles in natural fractures, we used a high-precision three-dimensional scanner to scan the natural fracture surface. The flow space of natural fracture was reconstructed with the combination of reverse engineering modelling technology and scan results. Based on the CFD-DEM method, the particle migration model of naturally fractured formation was established to investigate particles' migration, bridging and destabilization behavior in the wedge fracture space. The results show that the particle bridging position and bridging form is closely related to the fracture aperture and the particle size. The typical particle bridging structures are single-grain and double-grain, and the fracture deformation could induce the particle bridging structures to vary from single-grain bridging to double-grain bridging. The seal process is a dynamic process of repeating bridging seal, bridging destabilization, re-migration, bridging and seal again. There are a large number of strong force chains at the bridging particles in the leading edge of the seal zone, which are the foundation for forming the seal zone. The force chain network gradually weakens from the front to the entrance direction. This research provides a better insight into the process of fracture sealing by granular LCMs, which indicate that irregularity of the natural fracture aperture has a crucial effect on the structure and position of particle bridging.

Keywords Spatial reconstruction · Particle bridging · Force chain network · Dynamic evolution

J. Feng · G. Li (✉) · R. Li · Y. Zhang
State Key Laboratory of Oil and Gas Reservoir Geology and Exploration, Southwest Petroleum University, Chengdu 610500, Sichuan, China
e-mail: ligao@swpu.edu.cn

S. Li (ed.), *Computational and Experimental Simulations in Engineering*, Mechanisms and Machine Science 146, https://doi.org/10.1007/978-3-031-44947-5_99

1 Introduction

In the exploration and development of deep oil and gas resources, natural fractures are widely distributed, and the problem of lost circulation of drilling fluid has become one of the core bottlenecks that restrict the safety and efficiency of deep oil and gas reservoir drilling [1]. The existing plugging operations are often characterized by blindness and frequently face underground accidents such as difficulties in plugging once and repeated losses. The main reason for this is the inadequate understanding of the transport and bridging mechanisms of solid particles in natural fractures.

Previous research has conducted numerous studies on the issue of drilling fluid leakage and plugging mechanism in fractured formations. In terms of experimental research, Li et al. [2, 3] proposed a visualization plugging experimental apparatus based on reconstructed natural fractures to investigate the transport, bridging, and stacking behavior of particles with different mass concentrations and shapes in the natural fractures. They found that the concentration of particles exhibits a game phenomenon in the bridging behavior, where it is too low to reduce bridging efficiency, and too high to cause the closure of the fracture and decrease the plugging efficiency. Yang et al. [4], on the other hand, studied the transport and plugging process of solid fibers and particles in fractures through visualization experiments. These studies mainly analyzed macroscopic plugging behavior, lacking consideration of the interaction between rough natural fracture surfaces and solid particles, and revealing the mechanism remains insufficient. In terms of numerical simulation, CFD-DEM method has become a commonly used technique for studying the transport of particles in fractures. Zhu et al. [5] investigated the pressure drop, particle loss, particle trajectory, and contact force chain evolution law during the transport-bridging-stacking-plugging process of solid particles in a vertical fracture. Lee and Dahi Taleghani [6, 7] studied the efficiency of particle transport, bridging, and plugging in fractures by considering the impact of fluid viscosity, particle size, PSD, friction coefficient, and Young's modulus. However, these studies mainly placed smooth plane parallels or wedges to simulate the flow space of fractures, ignoring the true morphology and roughness of natural fractures, making it difficult to reveal the transport and bridging mechanism of solid particles in natural fractures at a microscopic level. Furthermore, in these studies, the deformation of fractures is completely ignored, which is the main cause of instability of bridging particles.

To address the shortcomings of the above research, we used a high-precision three-dimensional scanner to scan the natural fracture surface. The flow space of natural fracture was reconstructed with the combination of reverse engineering modelling technology and scan results. Based on the CFD-DEM method, the particle transport model of naturally fractured formation was established to investigate particles' transport, bridging and destabilization behavior in the wedge fracture space from a meso-perspective. Exploring the formation mechanism of the macroscopic plugging zone at a mesoscopic level can improve plugging technology and has significant implications for practical construction and production.

2 Construction of Particles Transport Model in Naturally Fractured Formations

2.1 CFD-DEM Method

The typical CFD-DEM coupling method is based on the Euler–Lagrange framework, which follows the coarse-grained fluid-particle coupling analysis method proposed by Tsuji et al. [8, 9]. On the one hand, the local averaging concept proposed by Anderson and Jackson [10] is used to handle the continuity equation and the N-S equation. The computational fluid dynamics (CFD) method is used to solve the fluid flow in the fluid element at the mesoscale. On the other hand, the discrete element method (DEM) is used to solve the motion law of solid particles at the mesoscale, where the particle motion is controlled by Newton's second law. The coupling between the two phase is achieved by considering the interaction between the fluid phase and the particle phase through the drag force model.

Fluid Phase Governing Equations

The flow of an incompressible fluid phase is governed by the locally-averaged version of the continuity equation and the N-S equation proposed by Anderson [10]. The governing equation can be described as follows:

$$\frac{\partial(\varepsilon_f)}{\partial t} + \nabla \cdot (\varepsilon_f \mathbf{u}_f) = 0 \tag{1}$$

$$\frac{\partial(\rho_f \varepsilon_f \mathbf{u}_f)}{\partial t} + \nabla \cdot (\rho_f \varepsilon_f \mathbf{u}_f \mathbf{u}_f) = -\nabla p - \mathbf{F}_{pf} + \nabla \cdot \boldsymbol{\tau} + \rho_f \varepsilon_f \mathbf{g} \tag{2}$$

where ε_f is the volume fraction of fluid cell, t is time in s, $\mathbf{u}_f$ is fluid velocity vector in m/s, ρ_f is fluid density in kg/m^3, p is fluid pressure in Pa, $\mathbf{F}_{pf}$ is the resultant force of fluid–particle interactions in N, $\boldsymbol{\tau}$ is the viscous force tensor, and $\mathbf{g}$ is the gravitational acceleration in m/s^2.

Particles Phase Motion Governing Equations

The particles' motion calculated by considering the influences of other particles, the natural fracture walls and other relevant forces applied on each particle. The motion of each individual particle comprises a rotational component and a translational component. The governing equations of particles motion which are following Newton's second law are expressed as follows:

$$\frac{\partial \vec{\mathbf{u}}}{\partial t} = \frac{\mathbf{f}_{mech} + \mathbf{f}_{fluid}}{m} + \mathbf{g} \tag{3}$$

$$\frac{\partial \mathbf{w}}{\partial t} = \frac{\mathbf{M}}{I} \tag{4}$$

where $\mathbf{u}$ is the particle velocity in m/s, m is the particle mass in kg, $\mathbf{f}_{mech}$ is the sum of additional forces acting on particle in N, $\mathbf{f}_{fluid}$ is the total force applied by the fluid on the particle in N, $\mathbf{w}$ is the particle angular velocity in rad/s, $\mathbf{M}$ is the moment acting on the particle in N m, I is the moment of inertia in kg m^2. $\mathbf{f}_{fluid}$ is made up of two parts: $\mathbf{f}_{drag}$ the drag force, $\mathbf{f}_{pg}$ force due to the fluid pressure gradient [10].

Fluid–Particles Interactions

The drag force is the main dynamics of particle motion, and also the most important force in two-phase coupling. Note that the fluid–particle interaction force is always applied at the particle centroid, and no rotational moment is applied to the particle. The drag force is defined as:

$$\mathbf{f}_{drag} = \mathbf{f}_d \varepsilon^{-\chi} \tag{5}$$

where $\mathbf{f}_d$ is the single particle drag force in N, $\varepsilon^{-\chi}$ is an empirical factor to account the local porosity. This correction term makes the force applicable to both high and low-porosity systems and for a large range of Reynolds numbers [10].

The resultant force of fluid–particle interactions is defined as:

$$F_{pf} = \frac{\sum_i^n \mathbf{f}_d}{V} \tag{6}$$

where V is the volume of the fluid element in m^3 and the sum is over the particles which overlap the fluid element.

The single particle drag force is defined as:

$$\mathbf{f}_d = \left(\frac{1}{2} C_d \rho_f \pi r^2 |\mathbf{u} - \mathbf{v}| (\mathbf{u} - \mathbf{v}) \right) \tag{7}$$

where C_d is the drag coefficient, r is the particle radius in m, $\mathbf{u}$ is the particle velocity in m/s, $\mathbf{v}$ is the fluid velocity in m/s. The drag coefficient is defined as:

$$C_d = \left(0.63 + \frac{4.8}{\sqrt{\mathrm{Re}_p}} \right)^2 \tag{8}$$

where Re_p is the particle Reynolds number.

The empirical coefficient is defined as:

$$\chi = 3.7 - 0.65 \exp\left(-\frac{\left(1.5 - \log_{10} \mathrm{Re}_p\right)^2}{2} \right) \tag{9}$$

The particle Reynolds number is defined as:

$$\mathrm{Re}_p = \frac{2\rho_f r|\mathbf{u}-\mathbf{v}|}{\mu_f} \tag{10}$$

where μ_f is the dynamic viscosity of the fluid.

The total force applied by the fluid on the particle id defined as:

$$\mathbf{f}_{fluid} = \mathbf{f}_d + \mathbf{f}_{\mu_f} + \mathbf{f}_{\nabla p} \tag{11}$$

where $\mathbf{f}_{\nabla p}$ is the force induced by pressure gradient on particle in N, $\mathbf{f}_{\mu_f}$ is the viscous force that fluid exerts on particle in N.

The force induced by pressure gradient on particle is defined as:

$$\mathbf{f}_{\nabla p} = \frac{4}{3}\pi r^3 \nabla p \tag{12}$$

where ∇p is the pressure gradient in Pa/m.

The viscous force that fluid exerts on particle is defined as:

$$\mathbf{f}_{\mu_f} = -\frac{4}{3}\pi r^3 \rho_f \mathbf{g} \tag{13}$$

2.2 Geometry Model of Natural Fracture

The formation of natural fractures is influenced by multiple factors, and their internal spatial morphology is difficult to quantify. It is time-consuming and has any universal significance to use a large number of natural fractures to reconstruct models. In this paper, in order to explore the behavior of particles' transport and bridging, we used a high-precision three-dimensional scanner to scan a carbonate rock containing natural fractures. The geometry of natural fracture surface was reconstructed with the scan result (see Fig. 1a), then the geometry model of natural fracture as established (see Fig. 1b).

2.3 Numerical Model of Particles Transport in Natural Fractures

The construction of the numerical model of particle transport in natural fractures is based on the above established geometric model, which is implemented in the DEM side, and considering both calculation accuracy and efficiency, the individual fluid mesh size which is set to 2 mm × 2 mm × 1 mm, meshing strategy of 65 × 40 × 3 was chosen for the simulation.

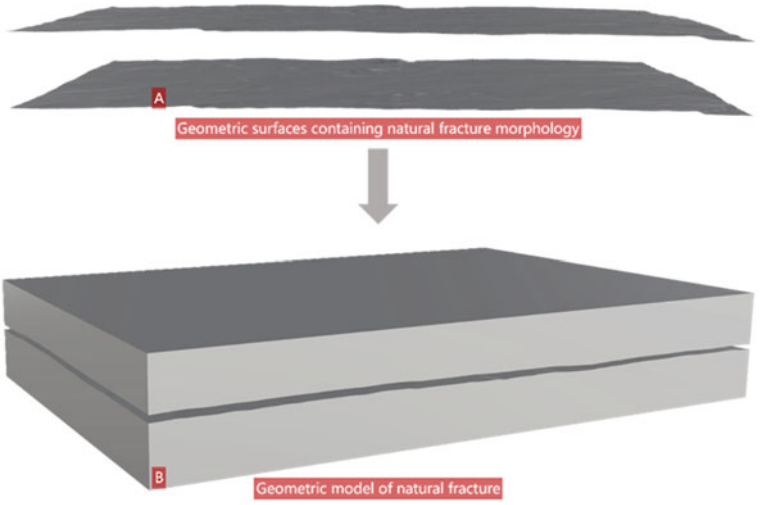

Fig. 1 Geometry model of natural fracture

The whole modeling process is shown in Fig. 2. It is worth noting that in order to facilitate the entry of particles into the fracture, a particle buffer zone is set at the left entrance of the model, where particles are generated and enter the fracture space under the action of fluid.

The coupled CFD-DEM model of the particle transport in natural fractures was developed and the process was shown in Fig. 3. At the beginning of the coupling process, a fluid mesh was created and the fluid parameters were set at the CFD side. This information is then transmitted to the DEM side, where the corresponding fluid calculation region is constructed. The particle motion within the current coupled timestep is then solved in the DEM side. The changes of the porosity and body force of each fluid grid caused by the particle motion are then transmitted back to the CFD side. Upon receiving this information, the CFD side began the next fluid calculation timestep and transmits the results to the DEM side, thus establishing a cycle of mutual information exchange between the two sides until the final solution of the two-way coupling of particle motion and fluid flow is achieved. It should be noted that the timestep in the DEM side is smaller than that in the CFD side, so in order to ensure temporal consistency, the DEM side is set to operate for 100 timesteps while the CFD side operates for only one timestep.

3 Result and Discussion

Particles transport simulations with different particle sizes and differential pressure were carried out base on the developed model. The basic properties of sphere and fluid are show in Table 1 and some other parameter show in Table 2.

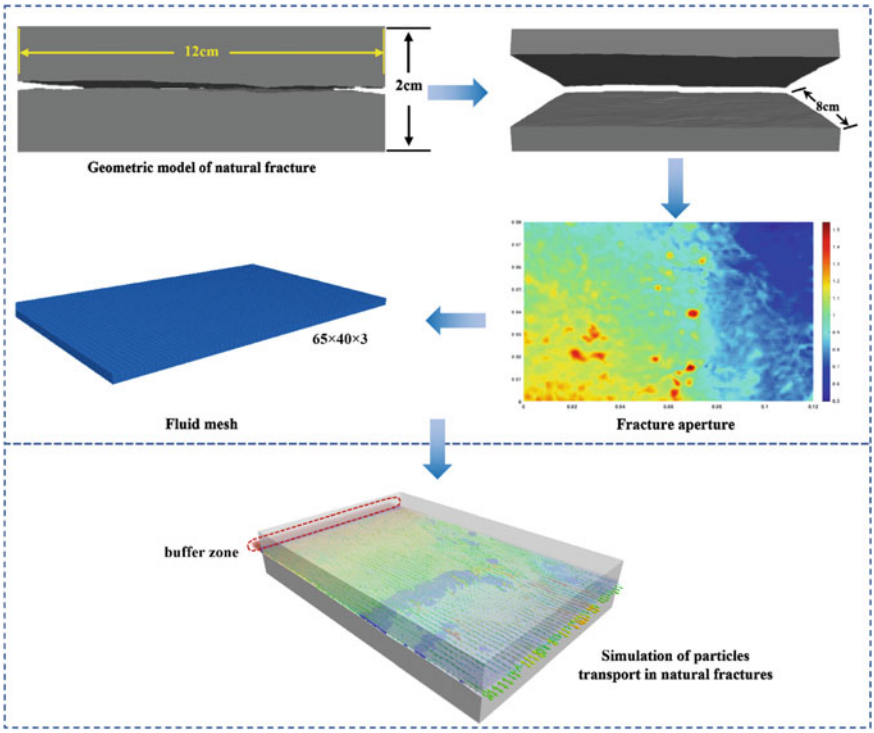

Fig. 2 Flow chart of CFD-DEM coupling model construction

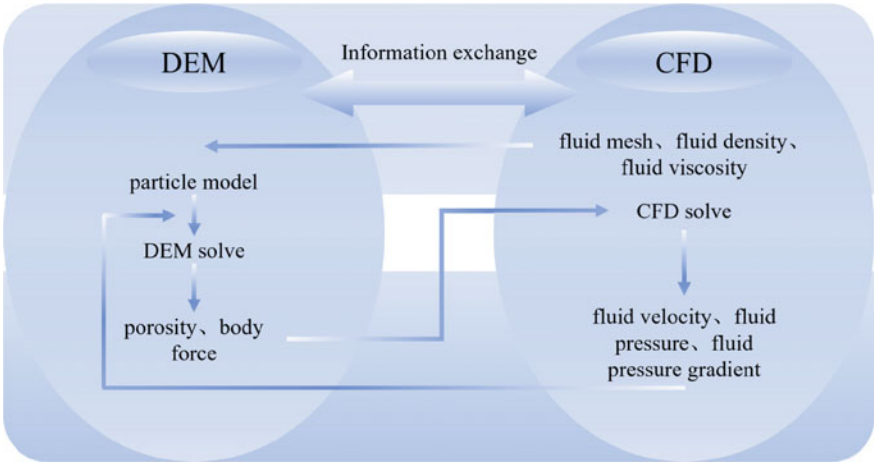

Fig. 3 CFD-DEM two-way coupling principle diagram

Table 1 Parameters of the fluid and particle in the proposed model

Phase	Property parameter	Value
Fluid	Fluid type	Incompressible Newtonian fluid
	Density (kg/m^3)	1400
	Dynamic viscosity (Pa s)	0.06
Particle	Density (kg/m^3)	1600
	Particle contact modulus (GPa)	1
	Friction coefficient between particles	0.5
	Friction coefficient between particles and fracture surface	0.5

Table 2 Parameters of different groups

Group number	Particle size (mm)	Inlet pressure (MPa)	Outlet pressure (MPa)
Group 1	0.4–0.5	0.1	0
Group 2	0.5–0.6	0.1	

3.1 Analysis of the Transport and Bridging Behavior of Particles in Natural Fractures

The transport behavior of particles in fractures plays a critical role in determining the formation and evolution characteristics of the seal zone. Particle transport in the fractures can be categorized into three distinct types: transport, bridging, and accumulation. With the combined effect of fluid flow, inter-particle collisions, and particle–wall interactions, particles transport in the fracture space. When the aperture of the fracture changes, particles are no longer able to go through smoothly and bridging. The followed particles were trapped in the place where bridging occurs. This bridging behavior typically involves a single particle, although double and multiple particle bridging can also occur. Subsequent particles accumulate near the bridged particles under the effect of fluid flow, ultimately leading to the formation of a seal zone gradually.

The result of transport and bridging simulation for 0.4–0.5 mm size particles with 0.1 MPa differential pressure are shown below. The result reveals that at the early stage, the fluid flow in the fracture is relatively gentle (Fig. 5a), and the particles transport steadily from the fracture entrance into the fracture space with the action of the fluid. Some large particles preferentially bridging in the place where the fracture aperture decreased, but the bridging positions are scattered and unstable (Fig. 4a). These scattered bridging particles became unstable with the subsequent particle impact and continued to transport forced by the fluid. As more and more particles enter the fracture, the front particles gradually transport to the position with small fracture aperture, and bridging as these places. The bridging location is randomly distributed according to the fracture spatial characteristics. The bridge

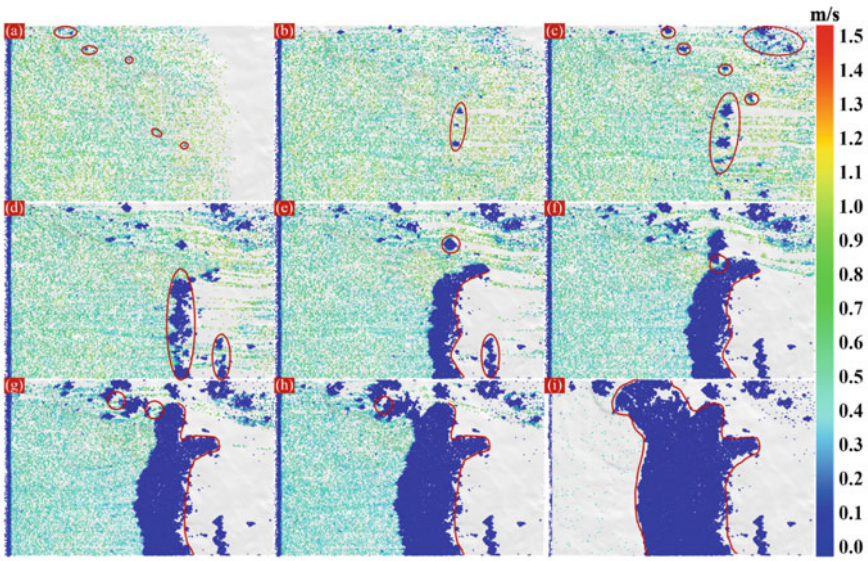

Fig. 4 Diagram of velocity for 0.4–0.5 mm size particles with 0.1 MPa differential pressure

structure formed here is more stable due to the smaller fracture aperture, and the fluid drag force and particle impact do not cause the bridge structure to collapse, but rather bring the bridge particles into closer contact with the fracture surfaces, making the bridge structure more stable (Fig. 4b).

With the formation of a stable bridging-building area, on the one hand, the bridging-building particles will occupy a part of the flow space of the fracture, narrowing the flow channel, which is conducive to "capture" particles and forming larger bridging area. A part of the particles that cannot bridging are lost through the channel, and the others will gradually accumulate around the bridging area (Fig. 4c, d). On the other hand, when the flow space of the fracture is occupied, the fluid velocity in the channel increases (Fig. 5c). The subsequent particles will impact the fracture surfaces and the particles already bridged under the action of the fluid drag force. In this process, the unstable bridging particles lose stability under the continuous impact of the fluid and particles, and the particles that are not affected become more stable. The seal zone skeleton area is gradually formed, and the local pressure increases with the formation of the seal zone skeleton area (Fig. 6c, d, f). Meanwhile, the increase of fluid velocity causes new particles faster to form new bridges or accumulations, and the bridges formed at this time are more stable than those formed at the beginning. The essence of this stage is the "screening" of stable bridging particles to form the seal zone skeleton area and the process of accelerate accumulation.

With the formation of the seal zone skeleton area, the fluid velocity decreases in the whole fracture space, but increases in the local area (Fig. 5d, e), which accelerates the bridging and accumulation of particles, while the destabilized bridging particles

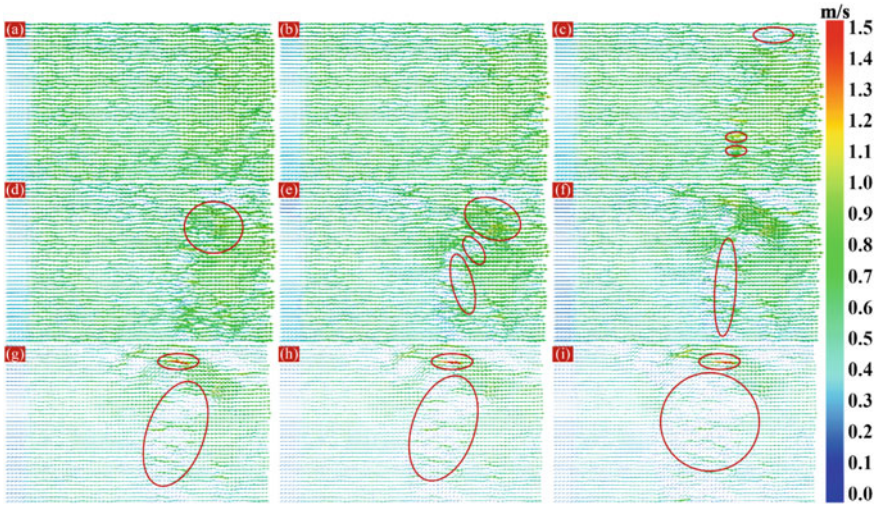

Fig. 5 Diagram of fluid velocity vector for 0.4–0.5 mm size particles with 0.1 MPa differential pressure

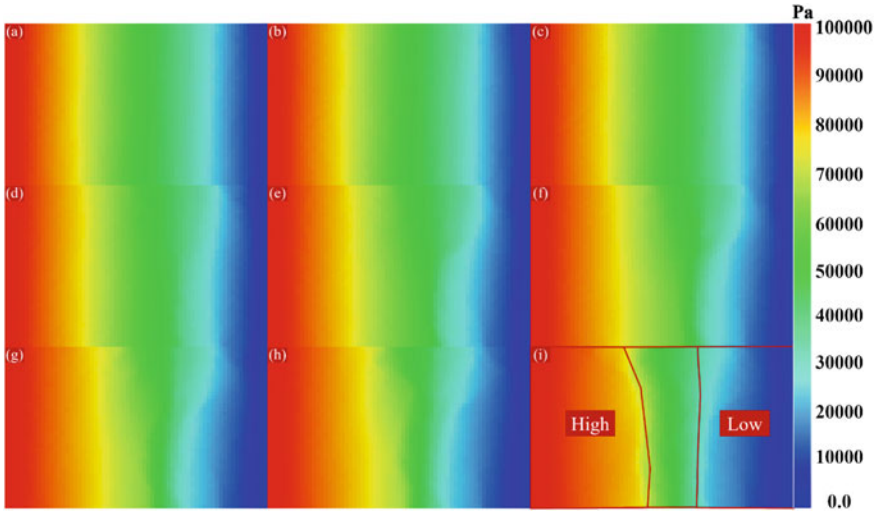

Fig. 6 Diagram of pressure for 0.4–0.5 mm size particles with 0.1 MPa differential pressure

are gradually lost (Fig. 5f). With the formation of the front of seal zone, the fluid velocity where with high value gradually slowed down with the subsequent particle bridging and accumulation (Fig. 5g), and the fluid velocity inside the stable seal zone reduced to a smaller value. At this moment, stop the new particles entering the fracture and the particles near the inlet side move toward the seal front with the fluid

drag force. After the formation of the seal zone, the bridging particles at the front of the seal zone bear the extrusion of the accumulated particles at the back side. If the bridging particles at the front are destabilized (Fig. 4g), the particles will continue to move along the destabilized gap of the seal zone (Fig. 4h) until new bridging particles are formed, and finally a stable and solid blocking layer is formed (Fig. 4i). The formation of a stable seal zone leads to an increase in pressure drop of the seal zone and divides the fracture space into roughly three regions, namely the near-inlet high-pressure zone, the seal zone, and the far-inlet low-pressure zone (Fig. 6i).

The simulation was carried out with the 0.5–0.6 mm size particles, and comparing the simulation results of 0.4–0.5 mm size particle, it can be found that a large number of large particles bridged at the fracture entrance and sealed the fracture entrance, resulting in only a small portion of particles could enter the fracture space (Fig. 7i). The bridging positions of the particles show a certain correlation with the distribution of fracture space aperture. This is due to the fact that as the particle size increases, the influence of the random distribution of fracture aperture in the local area of the fracture model on the bridging behavior of the particles is gradually highlighted, on the one hand, in the process of transport bridging, large particles form an effective bridging in a region with a small local crack opening, but due to the large variation of the surrounding fracture aperture, it is more difficult to form an effective bridging around it, and finally "traffic circle" type bridging accumulation occurs (Fig. 7f). On the other hand, it is difficult for large-sized particles to enter the position with a small fracture aperture, but they can only form effective bridging around these areas and complete certain accumulation, and finally appear "roundabout" type bridging accumulation (Fig. 7h). And because of the more dispersed location of the large size particle bridging, the distribution of high fluid velocity areas in the fracture space can be observed to vary with the bridging location (Fig. 8e–h), ultimately failing to form an effective seal zone, and the pressure drop in the fracture space varies less (Fig. 9i).

At the same time, combined with the diagram of the fracture aperture distribution, we can judge that two types of bridging are formed in the simulation results: single-grain bridging and double-grain bridging.

3.2 Analysis of the Formation and Evolution of the Force Chain Network

The contact force could be formed by the collision and extrusion between particles and the fracture surface, which could be transmitted along the contact normal direction of particles. The stability of the force chain network is the basis for the ability of the seal zone to withstand external loads [11]. At the beginning, the particles enter the fracture space and a few scattered bridges are formed, at which point some force chains are formed (Fig. 10a), but these are weak and scattered. As the particles move to areas with less fracture aperture, a more stable bridge is formed and the strength

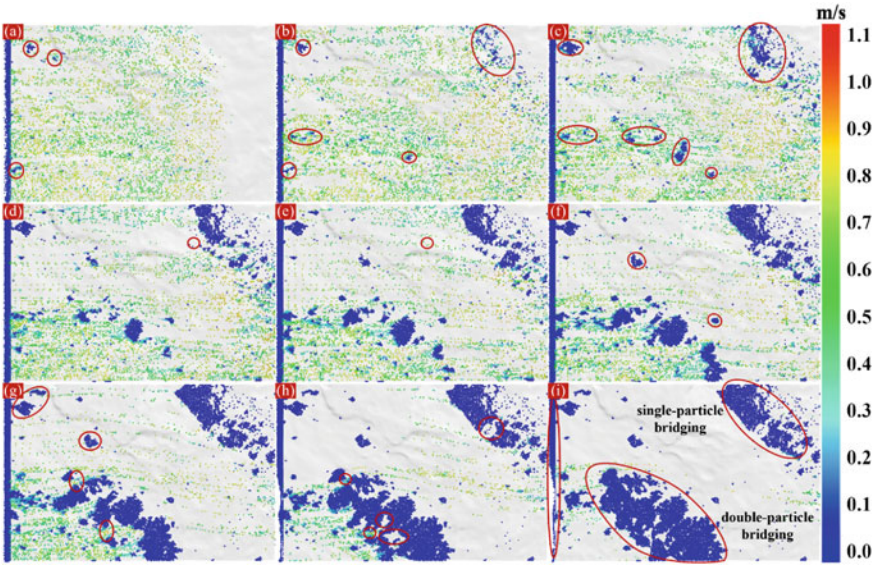

Fig. 7 Diagram of velocity for 0.5–0.6 mm size particles with 0.1 MPa differential pressure

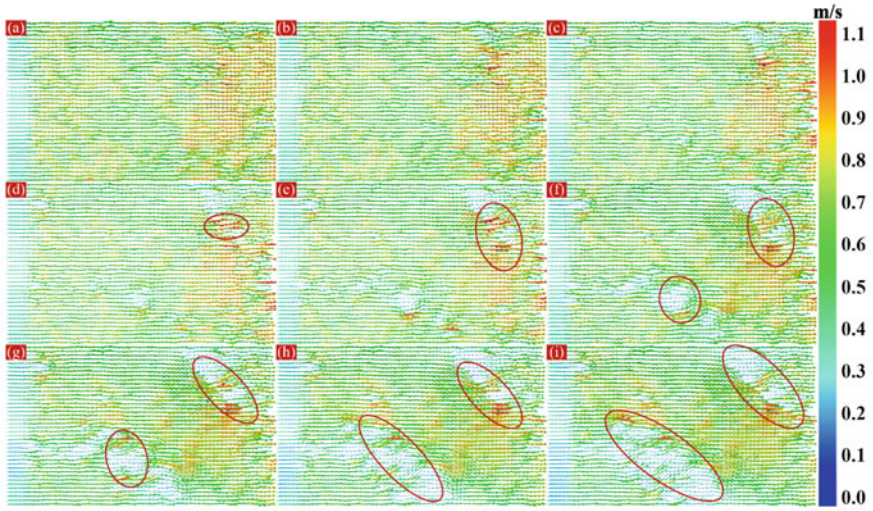

Fig. 8 Diagram of fluid velocity vector for 0.5–0.6 mm size particles with 0.1 MPa differential pressure

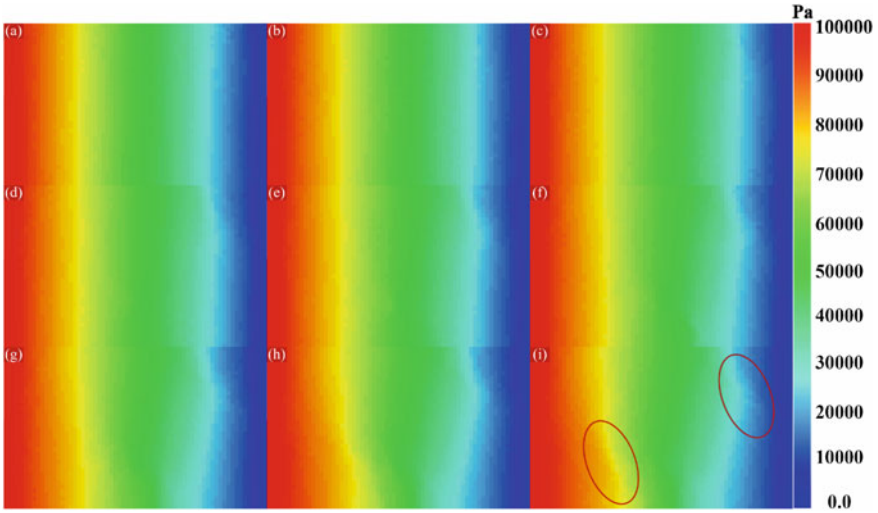

Fig. 9 Diagram of pressure for 0.5–0.6 mm size particles with 0.1 MPa differential pressure

of the force chains increases (Fig. 10b). However, the force chains are still small and dispersed and do not form a network of force chains. As the particles move further, the force chain network begins to develop as the particles build up around the force chain particles, and the small force chain network that has been formed continues to expand, with new bridging particles forming new force chains and then developing into a small force chain network (Fig. 10c). As the particles continue to bridge and accumulate, the individual small force chain networks interconnect to form an overall blocking skeleton force chain network (Fig. 10d). This is the basis for the formation of the blocking zone, with the contact between the skeletal particles and the fracture surface forming strong chains spread across the front of the blocking zone, supporting the further expansion of the blocking zone (Fig. 10f). The contact forces generated by subsequent particle accumulation are much less than those generated between the bridging skeletal particles and the fracture face, so the force chain network shows a trend of decreasing stress from the sealing front towards the fracture entrance (Fig. 10i).

The evolution law of the force chain network during the transport bridging of large size particle is similar to that of smaller particle. It should be noted that there are two bridging modes, single particle bridging and double particle bridging, in the results of large particle size. The force chain evolution reveals that the leading edge of the force chain network formed by double-particle bridging is stronger than that of single-particle bridging. This is because the fracture aperture is relatively large at the position where double-particles bridging is formed, which caused the accumulation of particles, i.e., the leading-edge particles are not only subjected to the resistance force of the wall, the drag force of fluid, but also the pressure transmitted by the accumulation of particles at the back end. However, in the position where single

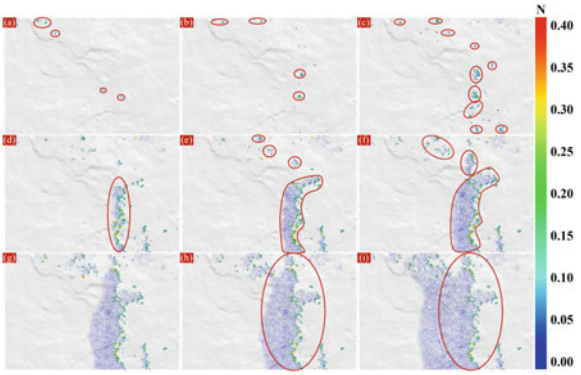

Fig. 10 Diagram of force chain for 0.4–0.5 mm size particles with 0.1 MPa differential pressure

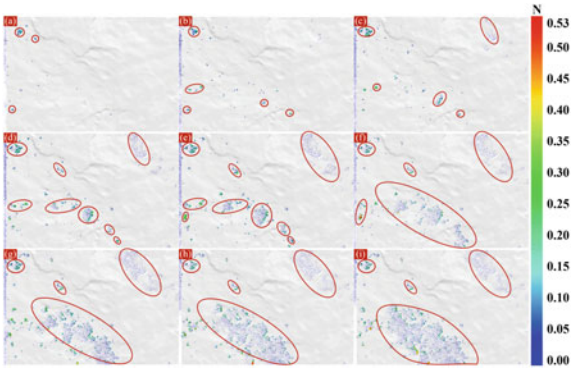

Fig. 11 Diagram of force chain for 0.5–0.6 mm size particles with 0.1 MPa differential pressure

particle bridging is formed, the fracture aperture is relatively small, and it is difficult for particles to accumulate. The single particle bridging in this area are only subjected to the two former forces, so the value of single particle bridging force chain is less than that of double particle bridging (Fig. 11).

4 Conclusion

(1) A two-phase flow model of natural fractured formations was established using the CFD-DEM method to obtain detailed information on particle velocity, fluid velocity, pressure, and contact force chains during particle transport. This provides a feasible approach for investigating the formation of macroscopic fracture sealing zones from a mesoscopic perspective.

(2) The position and form of particle bridging are closely related to the fracture aperture size and particle size, and bridging causes an increase in fluid velocity around bridging particles, resulting in increased drag force on the particles.

The sealing process is a dynamic cycle of repeated particle bridging, bridging destabilizing, re-transport, and further bridging.

(3) Strong force chains are observed at the front edge of the sealing zone, providing the foundation for sealing zone formation. The force chain network weakens gradually from the sealing front towards the inlet direction.

References

1. Li, X., Ji, H., Chen, L., Li, M., Xu, K., Jiang, X., et al.: Hydraulic fractures evaluation of the glutenite and the effects of gravel heterogeneity based on cores. Int. J. Rock Mech. Min. Sci. **160**, 105264 (2022)
2. Li, R., Li, G., Feng, Y., Yang, X., Teng, Y., Hu, Y.: Innovative experimental method for particle bridging behaviors in natural fractures. J. Nat. Gas Sci. Eng. **97**, 104379 (2022)
3. Feng, Y., Li, G., Meng, Y., Guo, B.: A novel approach to investigating transport of lost circulation materials in rough fracture. Energies **11**(10), 2572 (2018)
4. Yang, C., Zhou, F., Feng, W., Tian, Z., Yuan, L., Gao, L.: Plugging mechanism of fibers and particulates in hydraulic fracture. J. Petrol. Sci. Eng. **176**, 396–402 (2019)
5. Zhu, B., Tang, H., Wang, X., Zhao, F., Yuan, X.: Coupled CFD-DEM simulation of granular LCM bridging in a fracture. Part. Sci. Technol. (2019)
6. Lee, L., Dahi Taleghani, A.: Simulating fracture sealing by granular LCM particles in geothermal drilling. Energies **13**(18), 4878 (2020)
7. Lee, L., Dahi Taleghani, A.: The effect particle size distribution of granular LCM on fracture sealing capability. In: SPE Annual Technical Conference and Exhibition, Oct 2020. OnePetro (2020)
8. Tsuji, Y., Kawaguchi, T., Tanaka, T.: Discrete particle simulation of two-dimensional fluidized bed. Powder Technol. **77**(1), 79–87 (1993)
9. Tsuji, Y., Tanaka, T., Ishida, T.: Lagrangian numerical simulation of plug flow of cohesionless particles in a horizontal pipe. Powder Technol. **71**(3), 239–250 (1992)
10. Anderson, T.B., Jackson, R.O.Y.: Fluid mechanical description of fluidized beds. Equations of motion. Ind. Eng. Chem. Fundam. **6**(4), 527–539 (1967)
11. Yan, X., Xu, C., Kang, Y., Shang, X., You, L., Jing, H.: Mesoscopic structure characterization of plugging zone for lost circulation control in fractured reservoirs based on photoelastic experiment. J. Nat. Gas Sci. Eng. **79**, 103339 (2020)